Mon. Not. R. Astron. Soc. **000**, 1–16 (0000) Printed 13 March 2012 (MN LATEX style file v2.2)

Ultra Deep Catalogue of Galaxy Structures in the COSMOS field

Ilona K. Söchting[1⋆], Georgina V. Coldwell[2,3], Roger G. Clowes[4], Luis E. Campusano[5], Matthew J. Graham[6]

[1] *University of Oxford, Astrophysics, Denys Wilkinson Building, Keble Road, Oxford OX1 3RH, UK*
[2] *Instituto de Ciencias Astronómicas, de la Tierra y del Espacio, CONICET, San Juan, Argentina*
[3] *Univeridad Nacional de San Juan, San Juan, Argentina*
[4] *Jeremiah Horrocks Institute, University of Central Lancashire, Preston PR1 2HE, UK*
[5] *Departamento de Astronomía, Universidad de Chile, Casilla 36-D, Santiago, Chile*
[6] *CACR, California Institute of Technology, Pasadena, CA 91125, USA*

13 March 2012

ABSTRACT

This paper presents a large sample of intermediate to high redshift galaxy groups and clusters detected using a fully automated search in the COSMOS field. The detection algorithm is based on density peak extraction from a density distribution sampled using Voronoi tessellation within overlapping slices in the photometric redshift space. The cluster catalogue contains 1780 structures covering the redshift range $0.2 < z < 3.0$, spanning three orders of magnitude in luminosity ($10^8 L_\odot < L_4 < 5 \times 10^{11} L_\odot$) and richness from eight to hundreds of galaxies. All clusters at $z > 0.4$ and many even below this threshold show very prominent substructure indicating that $z \sim 0.4$ marks the slow emergence of virialized clusters in this field in agreement with published findings in other areas. The redshift distribution of detected structures shows strong variations with prominent peaks suggesting the presence of large scale structures across the whole range covered by this catalogue. Supercluster candidates have been identified at redshifts $z = 0.35$, 0.72, 0.94, 1.12, 1.27, 1.45, 2.0 and 2.52. At $z = 2.9$ we identified a compact agglomeration of galaxy groups and clusters suggesting the presence of another supercluster-like structure which would be the highest redshift candidate so far. Out of the nine supercluster candidates found in this study, six are new detections.

Key words: galaxies: clusters:general – catalogues – methods: statistical.

1 INTRODUCTION

Groups and clusters of galaxies are the largest gravitationally bound systems in the Universe. Their number density and clustering strongly depend on cosmological parameters providing potential means to constrain the underlying cosmological model (e.g Schuecker et al. 2003, Bahcall et al. 2003, Gladders et al. 2007, Rozo et al. 2009). Groups and clusters also harbour a large fraction of all galaxies and provide the vibrant environment that promotes their chemical evolution and morphological transitions. Consequently, the analysis of the group and cluster environment and its impact on the member galaxies fosters the understanding of the physical processes governing galaxy evolution and provides further testing of current models (Voit 2005).

The wealth of physical processes taking place in groups and clusters is exploited in the multiplicity of the group/cluster detection techniques. The most popular techniques include the detection of x-ray emission from hot gas (Romer et al. 2001, Pierre et al. 2006, Finoguenov et al. 2007), Sunyaev-Zel'dovich effect in the cosmic microwave background (Carlstrom et al. 2002, Voit 2005), cosmic sheare due to weak gravitational lensing (Weinberg & Kamionkowski, 2002), and galaxy overdensities in optical, NIR or mid-IR images (e.g. Koester et al. 2007, Lopes et al. 2004).

Abell (1958) constructed the first cluster catalogue by a systematic approach to the visual inspection of photographic plates. Zwicky et al. (1961–1968) constructed another large catalogue, also using visual inspection. Improvement of the performance and accessibility of computers allowed the implementation of fully automated cluster algorithms (e.g. Shectman 1985, Dodd & MacGillivray 1986). Since spectroscopic information is limited to very small areas of sky or to low redshifts (e.g $z \sim 0.15$ for the 2dFGRS, Colless et al. 2001), the challenge for cluster detection algo-

⋆ E-mail: iks@astro.ox.ac.uk

rithms is to reduce the projection effects using only photometric data. Postman et al. (1996) introduced a matched filter (MF) algorithm — a maximum-likelihood method, which assumes a filter for both the cluster radial profile and the luminosity function of the cluster galaxies. At the same time as improvements to the original MF resulted in the adaptive matched filter (AMF, Kepner et al. 1999), many other statistical and astronomical concepts found applications in galaxy cluster surveys. Voronoi tessellation (VT) has been applied very successfully in connection with thresholding of the density peaks (Ramella et al. 2001, Söchting, Clowes & Campusano 2002, Kim et al. 2000), or incorporating a maximum likelihood estimator (MLE, Söchting, Clowes & Campusano 2004, Söchting et al. 2006).

The deep multiwavelength data of the 2-deg^2 Cosmic Evolution Survey (COSMOS; Scoville et al. 2007) opens the opportunity for systematic searches for galaxy groups and clusters probing the deepest redshift yet. Knobel et al. (2009) compiled a spectroscopic group and cluster catalogue reaching $z \sim 1$. Finoguenov et al. (2007) used a combination of x-ray and photometric redshifts to reach $z \sim 1.3$. Taking advantage of new and much improved photometric redshifts published for galaxies in the COSMOS field by Ilbert et al. (2009), we present in this paper currently the deepest sample of groups and clusters reaching the redshift of $z \sim 3$.

The cosmological parameters adopted throughout this paper are: $\Omega = 0.3$, $\Omega_\Lambda = 0.7$ and $H_0 = 70$ kms^{-1} Mpc^{-1}.

2 DATA

We use the data of the 2-deg^2 Cosmic Evolution Survey (COSMOS; Scoville et al. 2007) with the 30-band photometric redshifts by Ilbert et al. (2009). The multi-wavelength COSMOS catalogue includes 607,617 objects and it was designed for studies of galaxies and large scale structures at high redshift. The data reaches a usable depth of $z = 3$ with sufficient objects at this redshift to allow statistically meaningful search for galaxy structures. According to Ilbert et al. (2009), the comparison of the derived photo-z with 4148 spectroscopic redshifts (i.e. $\Delta z = z_s - z_p$) indicates a dispersion of $\sigma_{\Delta z}/(1+z_s) = 0.007$ at $i^+_{AB} < 22.5$; at fainter magnitudes $i^+_{AB} < 24$ and $z < 1.25$, the accuracy is $\sigma_{\Delta z}/(1+z_s) = 0.012$. At higher redshifts ($z \sim 2$) the accuracy drops to $\sigma_{\Delta z}/(1+z_s) = 0.06$ at $i^+_{AB} \sim 24$.

As shown in Figure 1, the relative depth of the coverage changes dramatically over redshift with the lowest redshifts being dominated by very high numbers of low luminosity galaxies. Thus, the input galaxy catalogue used to construct the cluster search was restricted in magnitude ($i^+_{AB} < 21.5{+}3.0{\times}z_{ph}$) to avoid over-saturation at lower redshifts by small dwarf galaxies. The choice of the parameters was driven by the desire to construct a relatively homogeneous input catalogue up to the redshift of $z \sim 1.3$ which marks the start of more rapid degradation of the accuracy of the photometric redshifts of the input data. Note that this restriction doesn't have any impact beyond $z \sim 1.3$ where the selection limit matches the survey depth limit.

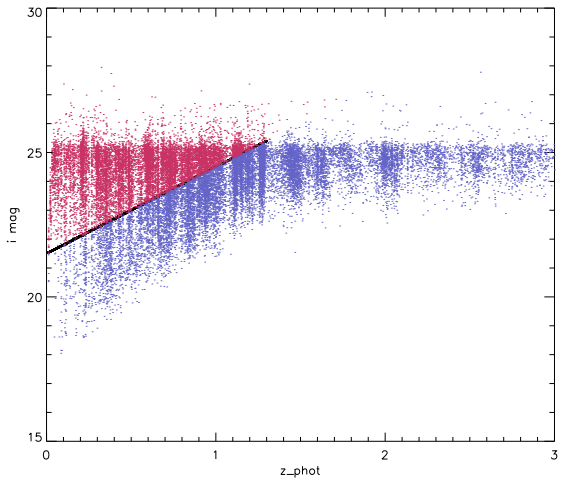

Figure 1. The i^+_{AB} magnitude distribution as a function of the photometric redshift with objects marked red (all objects above the solid line) being removed to improve the homogeneity of the depth coverage for the whole redshift range of our study. The solid line marks the threshold $i^+_{AB} < 21.5 + 3.0 \times z_{ph}$.

3 GROUP DETECTION ALGORITHM

The galaxy groupings are detected as density peaks in narrow slices in photometric redshift. The redshift slices are relatively narrow with $\delta z = 0.02 \times (1+z)$ and 50% overlap between the slices. The choice of the width of the redshift slices was based on $1\sigma = 0.01$ photometric redshift error found for faint COSMOS galaxies with infrared counterparts (Ilbert et al. 2009). The overlap is important to account for structures that would fall on to the boundary of two redshift slices. The size of the COSMOS field is very small relative to typical sizes of rich galaxy clusters at the lowest redshift ($z < 0.2$), compromising their detection. For this reason, the detection procedure was started at $z = 0.18$ resulting in a catalogue biased against clusters at $z < 0.2$.

In each redshift slice, the density distribution was sampled using a Voronoi Tessellation (VT) by application of IDL routines *triangulate* and *vornoi*. VT provides a partition of the investigated area into convex cells around every galaxy (Figure 2). The inverse of the area of a Voronoi cell gives the number density at the position of the galaxy. Since only the spatial structure of the galaxy distribution decides the sizes of the cells, VT provides a non-parametric method of sampling the underlying density distribution. For more information on Voronoi tessellation see Okabe et al. (2000) and references therein.

Galaxy clusters are detected as peaks in the galaxy density (δ) distribution. The simplest approach to locate the density peaks is to select objects that exceed a threshold σ for the density contrast with respect to the background. The density contrast σ_i at the position of the ith object is defined as

$$\sigma_i = (\delta_i - \bar{\delta})/\bar{\delta}, \quad (1)$$

where δ_i is the density and $\bar{\delta}$ is the mean density. One should remember that using Voronoi cells the mean density is calculated as

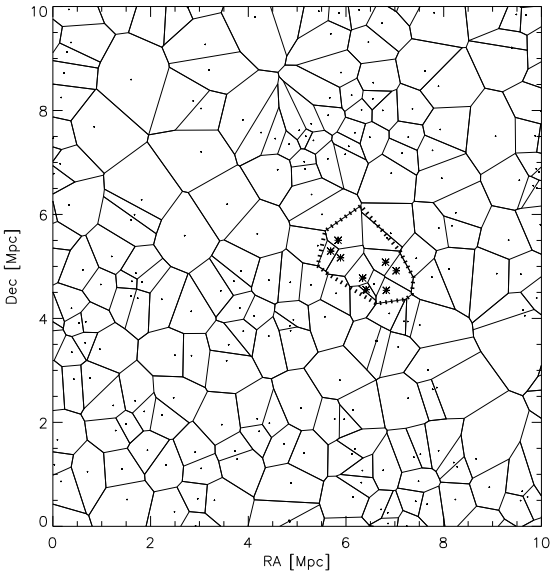

Figure 2. Example of Voronoi tessellation constructed on the actual data from a slice at $z \sim 2.7$ around a poor cluster (ID 1758) at the limit of our detection criteria (8 members). The black dots are galaxies within the redshift slice ($2.667z2.816$) and the asterisks are members of the cluster. The dotted polygon is the boundary of the cluster (see later sections for details).

$$\bar{\delta} = \frac{1}{n} \sum_{i=1}^{n} \frac{1}{A_i} \tag{2}$$

where A_i is the area of the Voronoi cell around object i and n is the overall number of objects. This approach has been applied in most VT-based procedures, producing excellent results (e.g. Ramella et al. 2001, Söchting, Clowes & Campusano 2002, Kim et al. 2000).

Candidate structures are selected in each redshift slice as density peaks above twice the mean density ($\sigma = 1.0$) with a minimum of eight connected cells exceeding the density limit. The limit of eight minimum members is born out of our previous experience of using Voronoi Tessellation for cluster detection and the desire to exclude the poorest structures. The samples from all the slices were combined by merging any structures with eight or more common members. This is a very conservative approach, adopted to practically eradicate over-merging (accidental merging of distinct and separate structures) and preserving self-contained subclusters of larger galaxy clusters as distinct structures. The main motivation is the lack of clarity as to when a group may or should be considered to be an integral part of a richer cluster and when it is just a close neighbour and member of the same supercluster. The risk associated with a conservative approach is occurrence of some fragmentation which is an undesirable splitting of bound components into separate structures. However, as shown in the later sections of this paper, our conservative approach preserved even forming clusters as single structures and separated out only groups very distinct from the main structures. We are mostly interested in the relation between galaxy structures and AGN and the composition of galaxy clusters and consequently have chosen an approach that best aids our research.

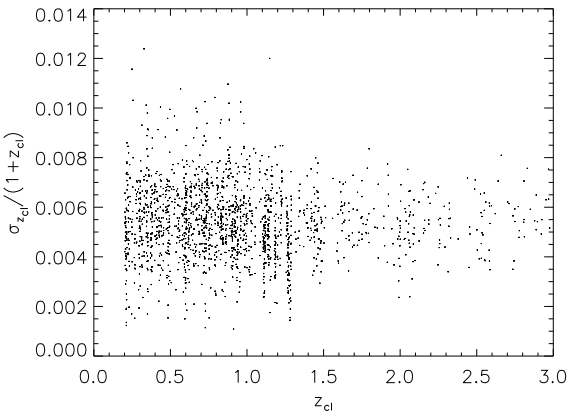

Figure 3. Distribution of the standard deviation of the photometric redshifts of member galaxies. Each point corresponds to a single galaxy cluster.

To ensure a homogeneous definition of richness and also to reduce the contamination by by-chance projections the final structure memberships have been limited to galaxies falling within $\pm 0.02 \times (1 + z_{cl})$ redshift region around the cluster redshift z_{cl}. A median redshift was used to calculate the z_{cl} to ensure the best possible centring in the redshift space with minimum impact by outliers which might have been merged due to projection effects. Only galaxies in the final membership selection are used to define the boundaries of the structures and compute structure parameters in the catalogue. The boundary of a structure is defined as a smallest convex hull (=polygon of minimum area) that encloses all the vertices of the voronoi cells of all the final cluster member galaxies as defined by the tesselation of all galaxies within the redshift slice $z_{cl} \pm 0.02 \times (1 + z_{cl})$. Such approach excludes galaxies that are simultaneously on the spatial and redshift edges of the original detection from influencing the determination of the cluster boundary.

4 EVALUATION OF THE CATALOGUE COMPLETENESS

Due to the degrading accuracy of the photometric redshifts and the decreasing relative depth of the COSMOS data at redshifts $z > 1.25$ (Ilbert et al., 2009), our catalogue is becoming increasingly biased against poorer structures beyond that redshift. The lack of comparable cluster samples in the literature and the uncertain nature of the structure evolution beyond $z \sim 1.0$ makes it impossible, for the time being, to provide a meaningful estimate of the catalogue completeness beyond this redshift. At the lower redshift, $z < 1$, the existing x-ray and optically selected cluster catalogues in this field provide a useful benchmark to test the completeness of our catalogue.

The x-ray selected sample of Finoguenov et al. (2007) contains 63 clusters at redshift $z > 0.2$. Assuming matching criteria demanding the quoted x-ray position to be within the boundary of a cluster in our sample and also within

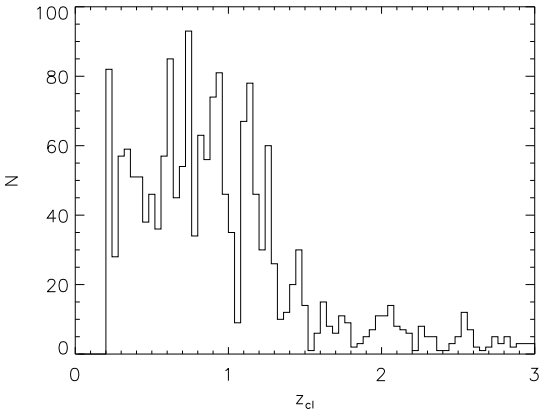

Figure 4. The redshift distribution of all groups and clusters included in our catalogue.

$\Delta z = 0.1$ in the redshift space, 56 of the x-ray clusters have counterparts in our catalogue. Looking closely at the possible non-detections, we found that two of the x-ray clusters (IDs: 3 and 9) are at the very edge of the field and lack proper optical sampling and the remaining five x-ray clusters (IDs: 93, 87, 20, 51, 134) are extremely weak x-ray detections and would fall outside the detection criteria in many other x-ray cluster selections. Thus, we conclude that our catalogue is $92 - 100\%$ complete relative to a x-ray selected catalogue.

The spectroscopically selected (zCOSMOS 10k galaxy sample) catalogue by Knobel et al. (2009) provides a useful comparison in optical regime up to $z \sim 1$. To match it with our compilation, it has been restricted to $z > 0.2$ and also the border line detections ($GRP = 0$ - usually very poor groups detected by a single method which failed verification by the second method) have been removed to provide the best "like with like" comparison. The remaining 536 clusters of the Knobel et al. sample have 308 objects (57%) in common within our catalogue if we use $d_r = 5$ arcmin and $\Delta z = 0.04$ as matching criteria. These criteria are different from those used for the x-ray selected catalogue because of the high accuracy of the spectroscopic redshifts used by Knobel et al. but poor cluster centring due to low membership numbers (in some cases just 2 member galaxies). Thus, we found that using a fixed search radius of $d_r = 5$ arcmin accounts better for the uncertainty of the cluster/group centres. Knobel et al. (2009) quote a purity parameter for their catalogue of $\sim 80\%$ which would suggest that our catalogue is at least 71% complete relative to the Knobel et al. sample. Conversely, 27% of $z < 1$ structures from this catalogue are also found in the Knobel et al. (2009) sample.

Taking advantage of the fact that all galaxies in the zCOSMOS 10k galaxy sample used by Knobel et al. have counterparts in the photomteric COSMOS sample used in our study, we also compared both cluster catalogues using shared member galaxies as a matching criterion. Without any restrictions applied to the Knobel et al. sample, we found that 31% of their structures have at least one member galaxy in common with a structure presented in this paper. Constraining the Knobel et al. sample to only structures that have at least one member galaxy with a galaxy purity parameter $GAP = 2$ (i.e. at least one member galaxy has two-way match between the both detection methods used by Knobel et al.), $z > 0.2$ and at least 3 members, we identify 49% of structures in common with our sample. For structures with 5 or more members, which are highlighted by Knobel et al. as relatively secure detections, the agreement with the cluster sample presented in this paper increases to 70%.

Considering that we have matched catalogues derived through different techniques the level of agreement is very high and compares well with fractions published for other cluster catalogues (e.g. Szabo et al. 2011; Knobel et al. 2009). The new catalogue with the addition of galaxy clusters at $z > 1.3$ provides a substantial enhancement to the existing samples.

5 PROPERTIES OF THE GROUP AND CLUSTER SAMPLE

5.1 Redshift distribution

The cluster catalogue contains 1780 structures ranging from galaxy groups to rich galaxy clusters. The majority of structures, 1485 systems, have been detected below the redshift $z < 1.3$. This rapid decline in the detection rate can be mainly attributed to the limited depth of the COSMOS data and strong degradation of the accuracy of photometric redshifts above this redshift threshold. The typical standard deviation of the photometric redshifts of all the group/cluster member galaxies is around $0.006 * (1 + z_{cl})$ (Figure 3). The redshift distribution shows strong local variations (Figure 4) indicating the presence of large scale structures at multiple redshifts.

The presence of such peaks in the redshift distribution is clearly identifiable even at higher redshifts despite reduced detection depth. Such large scale structures are formed by the cumulation of several groups and clusters of galaxies allowing us to suggest the possibility of the presence of supercluster candidates at redshifts $z = 0.21$, 0.35, 0.72, 0.94, 1.12, 1.25, 1.45, 2.0 and 2.55. Furthermore, we note that a coherent structure beyond the scale of a single cluster is present at redshift $z = 2.9$, the most distant candidate for a precursor of today's superclusters. We revisit the spatial properties of those redshift agglomerations in a later section of this paper.

5.2 Richness distribution

The richness of structures within our catalogue is defined as the number of galaxies within the boundary of the cluster and its redshift limits, thus, equals the number of the final member galaxies. This measure is relative and numerical comparison between clusters is only valid within this catalogue. Nevertheless, we intend to add in the future spectroscopic mass estimates for some of the clusters to allow a calibration of the mass to richness relation. The catalogue contains a very high number of structures due to the inclusion of galaxy groups and poor clusters with the aim to foster the study of structure formation. As shown in Figure 5, it is dominated by groups and poor clusters throughout the

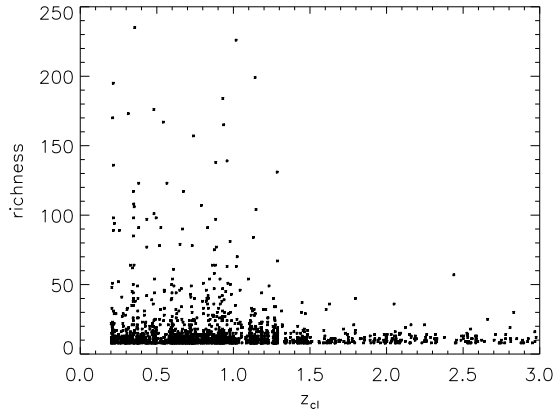

Figure 5. The distribution of richness vs redshift of all detected groups and clusters. The strong decline of the number of rich clusters beyond $z \sim 1.3$ could be an artefact due to the magnitude limit of the COSMOS data.

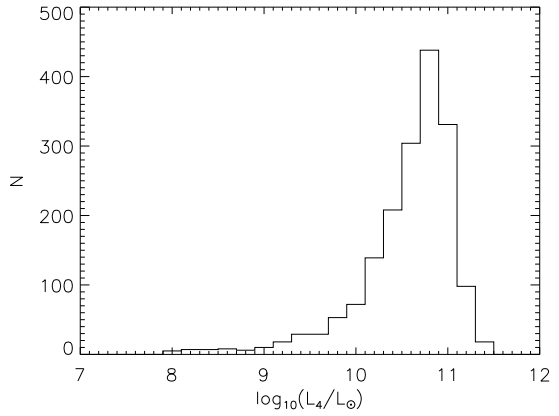

Figure 6. Histogram of the K band luminosities of groups and clusters in our catalogue approximated by the four brightest member galaxies.

whole redshift range up to $z \sim 1.3$, as would be expected in a hierarchical formation model. Beyond this redshift, the richness is increasingly underestimated due to the magnitude limit of the COSMOS survey, consequently, becoming a less satisfactory means of comparison for the detected structures.

5.3 Luminosity Distribution

Beside the richness, a second method to approximate the mass of a cluster is to use its luminosity. Nevertheless, it brings new challenges. Calculating the luminosity of a cluster as a sum of the luminosities of its member galaxies would assume that all members, down to the smallest dwarf galaxy, can be accounted for. Obviously, it is rarely the case and with increasing redshift a higher fraction of member galaxies must be assumed as undetected. At the low redshift, a fudge factor can be used with some success. However, with

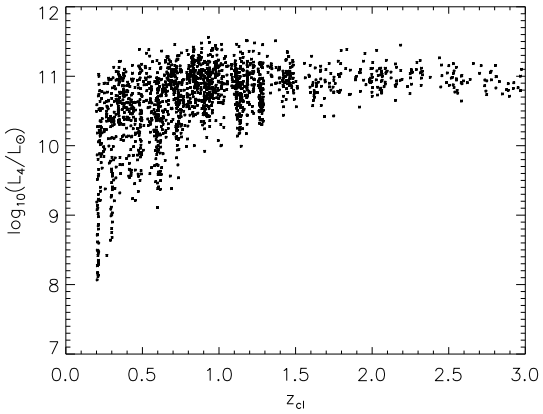

Figure 7. Redshift distribution of the K band luminosities of groups and clusters in our catalogue approximated by the four brightest member galaxies.

increasing redshift this approach is becoming highly inaccurate (Padilla et al. 2004). A different approach is to avoid the approximation of the total luminosity and use a constant number of brightest galaxies in every cluster to allow comparison between structures (but not the total mass approximation!). As outlined by Eke et al. (2004), such an approach might be in many cases more accurate than use of a virial estimate. Padilla, Lambas & González (2010) used the four brightest galaxies as a proxy and we adopted this approach to quote the K band luminosity for structures in this catalogue ($\sum_{i=4} L_i$ abbreviated as L_4 in the plots). The use of the limited number of the brightest galaxies in each structure addresses also the shortcoming of the richness measure which is increasingly underestimated for all structures at $z > 1.3$.

The K-band was chosen because the total stellar mass content is better reflected in the near-IR luminosities which are less influenced by the detailed star formation history of the galaxy. Also the shape of the near-IR spectral region is less dependent on the age of the stellar populations, and thus, the k-corrections. Consequently, the luminosities can be determined with larger precision in the K-band than in, for example, the V-band (Longhetti & Saracco, 2009). We used the classic k-correction assuming $z_f = 4$ and solar metallicity model (Bruzual & Charlot, 2003).

The catalogue covers over three orders of magnitude of cluster luminosities, ranging from $10^8 L_\odot$ to $5 \times 10^{11} L_\odot$ with the majority of structures in the $5 \times 10^{10} L_\odot$ to $10^{11} L_\odot$ range (see Figure 6).

Beyond the redshift of $z \sim 1.3$ structures with lower luminosities are disappearing due to the depth limit of the data. There is only a small decline in the peak luminosity with increasing redshift indicating that the most luminous cluster galaxies were already in place at the early stages of formation (Figure 7). The poorest structures span the widest range of luminosities and the richer structures converge to almost constant luminosities indicating that the more massive cluster galaxies have already formed at the group stage of cluster build-up (Figure 8).

Obviously, we need to verify that the presence of such

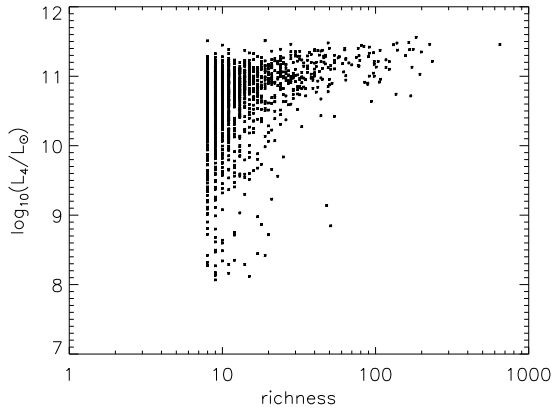

Figure 8. K band luminosity of groups and clusters versus their richness.

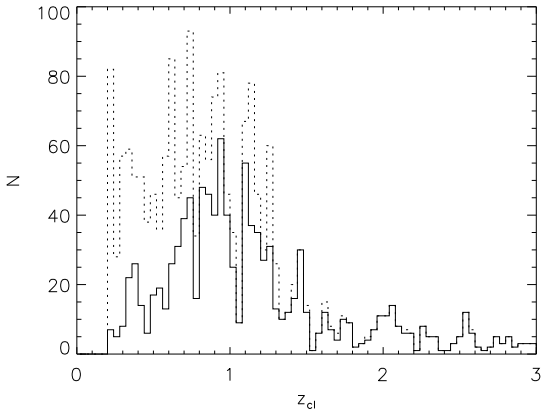

Figure 10. The redshift distribution of the bright structures ($\log_{10}(\sum_{i=4} L_i/L_\odot) > 10.7$) marked as solid line in relation to the overall sample (dotted line).

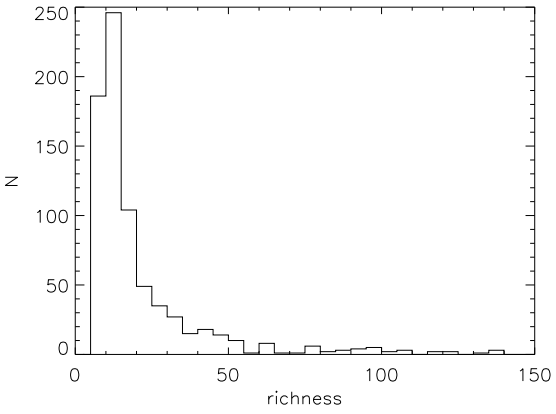

Figure 9. The histogram of the richness distribution of a sample restricted to just the brightest structures ($\log_{10}(\sum_{i=4} L_i/L_\odot) > 10.7$) at lower redshift ($z < 1.3$). The distribution appears dominated by very poor structures which verifies that the brightest cluster galaxies formed already at the group stage.

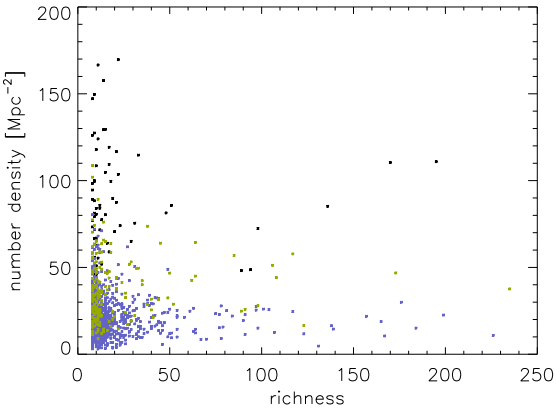

Figure 11. The distribution of density versus richness of all detected groups and clusters. The black, green and blue symbols indicate $z \leq 0.23$, $0.23 < z \leq 0.4$, $0.4 < z \leq 1.3$ structures respectively. It should be noted that the richness of $z > 1.3$ is underestimated and thus those structures have been omitted in the diagram.

very luminous groups and poor clusters is not a reflection of the underestimated richness of high redshift clusters. For this purpose, we plotted in Figure 9 the distribution of just the lower redshift ($z < 1.3$) high luminosity ($\log_{10}(\sum_{i=4} L_i/L_\odot) > 10.7$) structures. It shows clearly that even this restricted sample is strongly dominated by groups and poor clusters providing the needed verification.

Revisiting the redshift distribution with the cluster sample restricted to just the brighter objects ($\log_{10}(\sum_{i=4} L_i/L_\odot) > 10.7$), we notice that some of the low redshift peaks detected in the complete sample have disappeared (Figure 10). It seems that the structures at $z = 0.22$ and $z = 0.6$ are very numerous, however, lack very bright galaxies raising the question of how common such pseudo-superstructures consisting of groups and clusters of faint galaxies might be.

5.4 Density Distribution

The projected densities of galaxies in groups and clusters were calculated using the richness of the structures and their area defined as a convex hull enclosing all the Voronoii Tessells of the cluster members. The robustness of this approach to delineate the boundaries of galaxy clusters was illustrated by Söchting et al. (2002).

Figure 11 shows that surprisingly, not the richest but some of the poorest structures have the highest projected densities. The richest clusters, on the other hand, appear to favour the same projected number density with only a small fraction tracing the expected increase of density with richness.

Following those trends in more detail we find that the extremely dense but poor structures are almost all (39 out

of 43) associated with the $z = 0.21$ peak in the redshift distribution of all detected structures. Three others are associated with the next peak at $z = 0.29$ and a single one is at redshift of $z = 0.69$. Furthermore, all those extremely dense but poor structures are made up of relatively faint galaxies. One possible explanation would be a preferred direction in the distribution of small filaments in the $z = 0.21$ region which is plausible in the sense that it applies to a spatially very limited region and a very narrow redshift range. The extremely dense but poor structures would be simple projections of such filaments aligned with the line of sight. Other possibility would be that at low-redshifts, the regions with prominent large scale structure start to promote the creation of extremely compact groups of fainter galaxies, hardly present beyond $z = 0.3$.

Looking at the very rich structures tracing the constant density trend at around 20 Mpc^{-2}, we find that all those clusters are usually at somewhat higher redshift and have prominent substructure in form of filament-like overdensities extending in multiple directions (see Figure 12 for examples). On the other hand, structures following the trend of increasing density with increasing richness are all at the redshift of $z < 0.4$ and have little or weak substructure (see Figure 13 for examples). Thus, the trends visible in the projected density versus richness diagrams provide a genuine discrimination between rich but still forming clusters and evolved rich clusters. We note that clusters started to become evolved only very recently with all evolved clusters in the COSMOS field having redshifts $z < 0.4$.

6 SUPERCLUSTER CANDIDATES

The redshift distribution, presented in an earlier section, indicated the possible presence of 11 distinct layers of superstructures of which 9 can be considered as supercluster candidates on the basis of the presence of luminous clusters beside the enhanced overall number of structures. The three lowest redshift candidates have been already reported in literature (Knobel et al., 2007; Scoville et al., 2007). Also the pie diagrams of the RA v/s redshift and Dec v/s redshift distributions (Figures 14 and 15) indicate the presence of voids and agglomerations of luminous galaxy clusters. However, due to the uncertainty of the cluster redshifts based on just the photometric redshift of the member galaxies, a 3-D delineation and statistical verification of superclusters is at this point not possible. Basically, even assuming that all clusters have redshifts accurate to $0.006(1 + z_{ph})$, such error corresponds to much larger scale (30-150 Mpc) than the field size at the given redshift. Even an attempt to outline a 2D projected boundary of the superclusters is hamppered by the relatively small size of the COSMOS field. Einasto et al. (2011) found from a large sample of low redshift superclusters that their diameters range from about 20 to 100+ Mpch^{-1} and morphologies are usually very filametary. Considering that COSMOS field is just 20-40 Mpc in extend (redshift dependent), it is most likely covering just parts of the superclusters and to outline their boundaries, we would need to extend considerably its spatial coverage. Nevertheless, the current information allows us to visualise the presence of an assemble of galaxy clusters, which will be defined as supercluster candidates, at a level sufficient to mark them for future follow up.

A brief description of every supercluster candidate is presented in this paper and a detailed study of such structures will be shown in a future work.

z = 0.21 pseudo supercluster : The large overdensity of groups and clusters as the redshift $z = 0.21$ is dominated by very faint structures. This overdensity practically disappears when only bright clusters ($\log_{10}(\sum_{i=4} L_i/L_\odot) > 10.7$) are considered (Figure 10). For this reason we like to call it a pseudo supercluster. The structure is also unique in the sense that it contains numerous extremely dense groups. Those groups are relatively poor and faint and are found only very rarely outside the $z = 0.21$ pseudo supercluster. Figure 16 shows the spatial distribution of all groups and clusters within this structure. It should be noted that at this redshift the size of the COSMOS field is very small ($\sim$ 10 Mpc) in relation to known superclusters extending many tens of Mpc which could mean that only outskirts of a supercluster are covered.

z = 0.345 − 0.375 double layered supercluster : Two clear layers of groups and clusters occupy the same region and are separated only by $\Delta z = 0.03$ (Figure 17). Due to this proximity in the radial direction both structures could be part of the same supercluster. For clarity, Figures 18 and 19 show the distributions of groups and clusters in each layer separately.

z = 0.60 pseudo supercluster : The large overdensity of groups and clusters as the redshift $z = 0.60$ is dominated by very faint structures (Figure 20). This overdensity practically disappears when only bright clusters ($\log_{10}(\sum_{i=4} L_i/L_\odot) > 10.7$) are considered (Figure 10). Like the structure at $z = 0.21$, this agglomeration at $z = 0.61$ has been also classified as pseudo-supercluster.

z = 0.72 supercluster : This supercluster is dominated by a well known rich and luminous cluster $ID = 634$ at $z = 0.712$. The central cluster appears to be still in the process of formation as judged by the presence of filamentary substructure. As shown in the Figure 21, this is a highly dense and centrally concentrated supercluster candidate.

z = 0.94 supercluster : This supercluster candidate has somewhat broader redshift distribution, however, it consists of relatively luminous structures suggesting a strong mass enhancement. The projected 2-d distribution of groups and clusters in the redshift range of the supercluster (Figure 22) is also very non-uniform with a band of structures marking a local supercluster core.

z = 1.12 double − layered supercluster : Similar to the $z \sim 0.37$ supercluster candidate, this structure as well shows two clear layers of groups and clusters which occupy the same region and are separated only by $\Delta z = 0.02$ (Figure 23). Due to this proximity in the radial direction both structures could be part of the same supercluster.

z = 1.27 supercluster : A supercluster candidate consisting of luminous structures distributed in filamentary pattern towards a common point of origin (Figure 24). The member structures occupy a very narrow redshift range in particular considering the broadening introduced by the uncertainty of the photometric redshifts.

z = 1.45 supercluster : A prominent filament of bright groups and clusters extending along the Dec-axis (Figure 25).

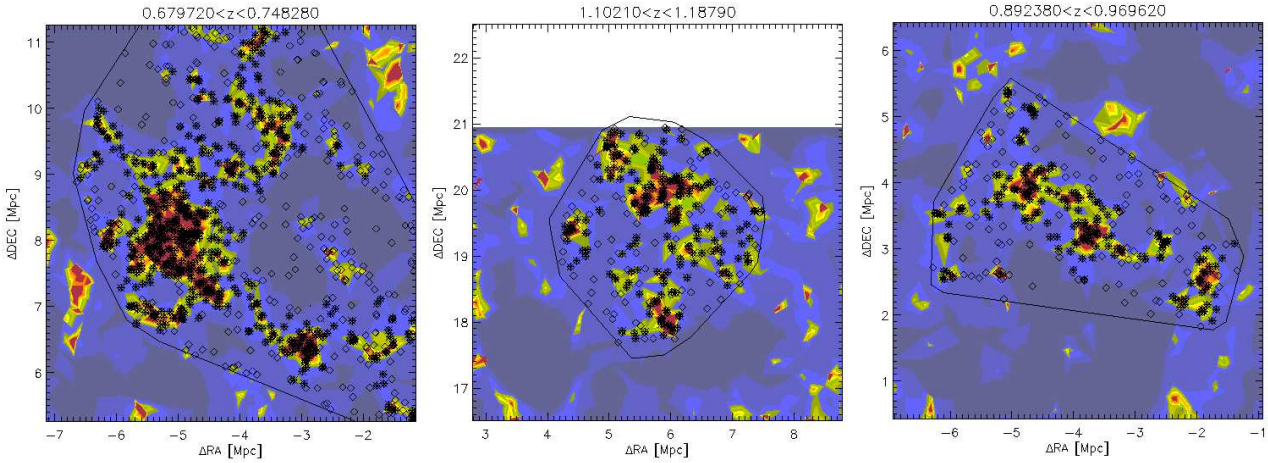

Figure 12. Examples of very rich clusters tracing the lower density branch of the density vs richness diagram. All such clusters have $z_{cl} > 0.4$. The contours indicate relative density distribution, the polygon outlines the boundary of the cluster and the asterisks mark the member galaxies.

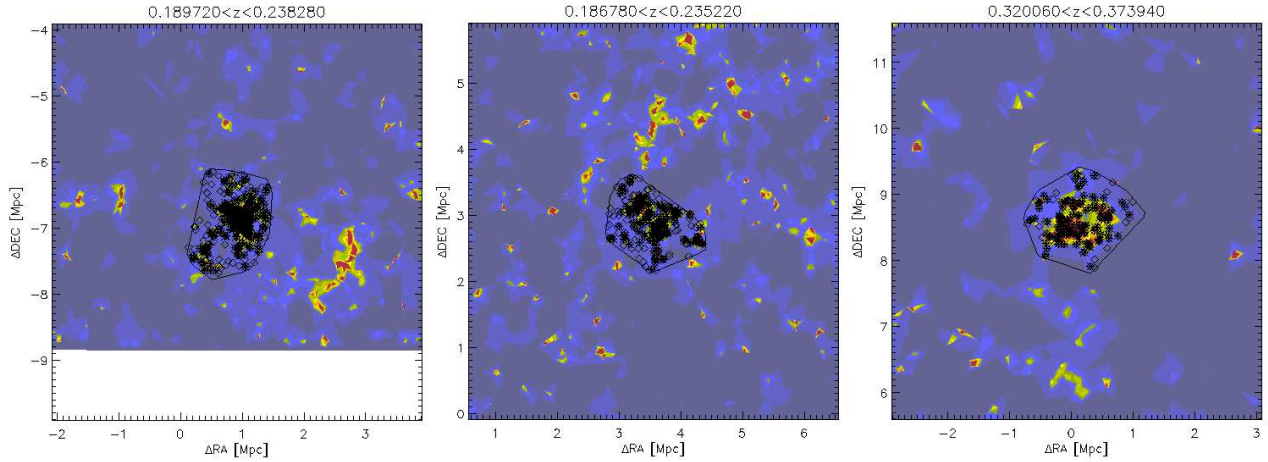

Figure 13. Examples of very rich clusters whose density correlates with richness. All such clusters have $z_{cl} < 0.4$. The contours indicate relative density distribution, the polygon outlines the boundary of the cluster and the asterisks mark the member galaxies.

z = 2.0 supercluster : This grouping of structures is fragmented in spatial and radial directions, however, the proximity of the fragments suggests that they might be connected within a single supercluster (Figure 26).

z = 2.52 supercluster : Agglomeration of luminous groups and clusters forming a diagonal filament in the RA-Dec and Dec-z_{ph} space (Figure 27) with increasing redshift at decreasing Declination.

z = 2.9 supercluster : This supercluster candidate has a broader redshift distribution but a very narrow and relatively small foot print in the RA - Dec plane.

7 CATALOGUE

The cluster catalogue contains 1780 structures covering the redshift range $0.2 < z < 3.0$, spanning three orders of magnitude in luminosity ($10^8 L_\odot < L_4 < 5 \times 10^{11} L_\odot$) and richness from eight to hundreds of galaxies. Table 1 lists the richest clusters providing an example of information available for all structures found by this study. The complete catalogue is published in the electronic version of this paper. The ID of the structure is the internal detection number. The RA and Dec are the mean coordinate of all the final member galaxies. The area of the structure is that of a smallest convex hull (=polygon of minimum area) that encloses all the vertices of the voronoi cells of all the final cluster member galaxies. The richness is the number of the final cluster members derived from the magnitude restricted input catalogue. The number density is the richness divided by area. The $\sum_{i=4} L_i$ is the sum of luminosities of the four brightest galaxies in the K band.

8 CONCLUSIONS

The presented catalogue of galaxy structures in the COSMOS field covers the redshift range $0.2 < z < 3.0$ which is currently the deepest compilation based on a fully automated detection algorithm. The included structures range

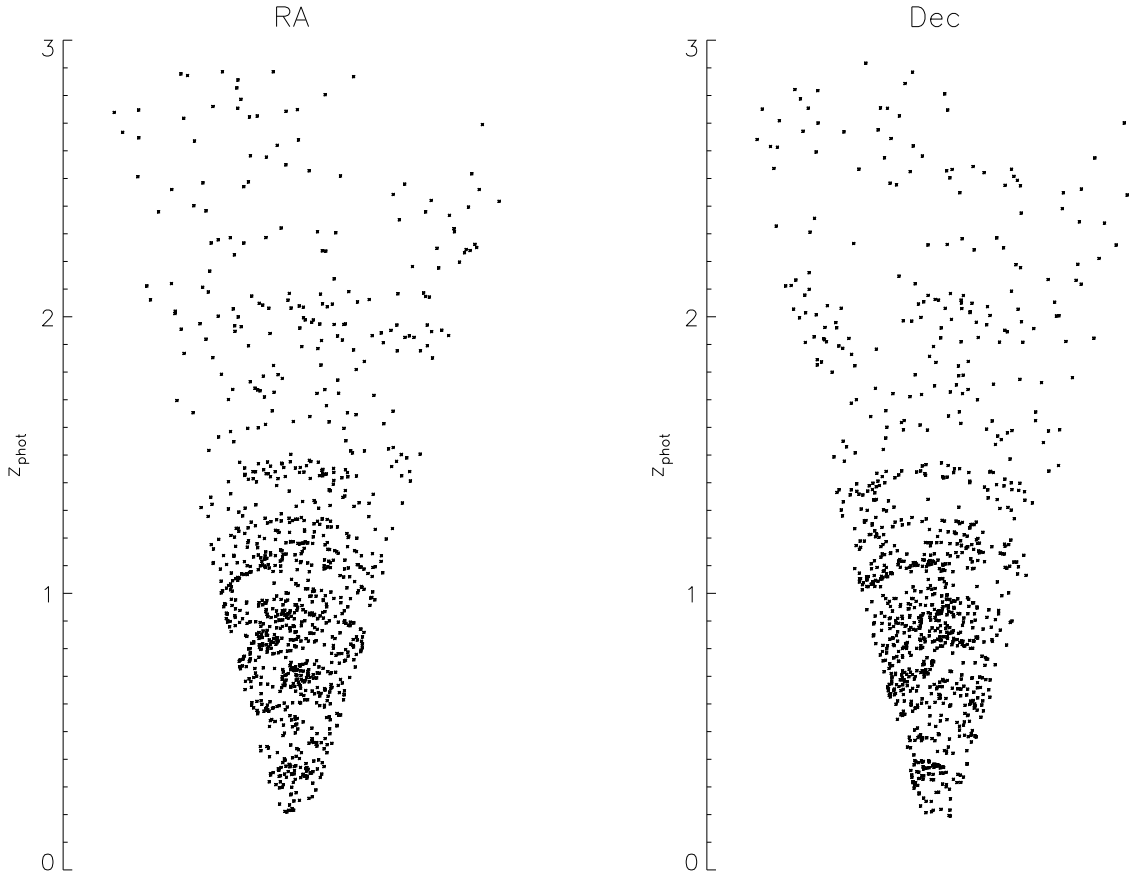

Figure 14. The large scale distribution of luminous galaxy clusters ($\log_{10}(\sum_{i=4} L_i/L_\odot) > 10.7$) galaxy clusters as the function of RA (left) and Dec (right).

from compact groups to rich clusters making it particularly well suited for the study of structure assembly with interesting results already emerging from the evaluation of the most basic sample parameters.

We find that a density versus richness diagram is a useful tool to discriminate between evolved clusters and those with still prominent substructure with the later showing lower densities relative to richness. According to this approach, morphologically evolved clusters with no or minimal signs of substructure are relatively recent appearance with all such structures within the COSMOS field having $z < 0.4$. It is compatible with the results of Maughan et al. (2008) who have studied the cluster morphologies in a large sample of 115 galaxy clusters in the redshift range 0.1 to 1.3 observed with Chandra and found a significant absence of relaxed clusters (as determined by centroid shift measurements) at $z > 0.5$. It is important to remember that our discrimination between evolved and forming clusters is based on the morphology, whereas, the sole presence of x-ray emission in connection with an overdensity of early type galaxies would suggest the presence of evolved clusters already at $z \sim 2$ (Gobat et al. 2011).

Numerous poor groups contain very massive galaxies as suggested by their $\sum_{i=4} L_i$ being only marginally smaller than that of the richest clusters. It would indicate that the most massive galaxies have already formed within groups and the clusters would have formed recently from the mergers of many compact groups and would still be in dynamically unrelaxed state, as suggested by Coziol et al. (2009). This scenario is also supported by our finding that all structures at $z > 0.4$ and many at the lower redshifts have prominent substructure and must be assumed as still forming.

Across the whole redshift range the numbers of structures appear to fluctuate forming strong local peaks suggesting the presence of large scale structures at many redshifts. The most prominent peaks are at redshifts $z \sim 0.35$, $z \sim 0.72$, $z \sim 0.94$, $z \sim 1.12$, $z \sim 1.27$, $z \sim 1.45$, $z \sim 2.0$, $z \sim 2.52$ and $z \sim 2.8$. The overdensities at $z \sim 0.35$ and $z \sim 0.72$ have been also detected by Knobel et al. (2009) and the $z \sim 0.94$ structure by Scoville et al. (2007). The $z = 0.72$ supercluster candidate is a well documented structure dominated by a rich galaxy cluster (ID634 in this study) previously discovered using weak-lensing method (Miyazaki et al. 2007) and also in x-ray (Finoguenov et al. 2007). The dominant cluster appears unrelaxed in the sense that it displays a lot of substructure. Nevertheless, the supercluster candidate is highly centrally concentrated around this cluster.

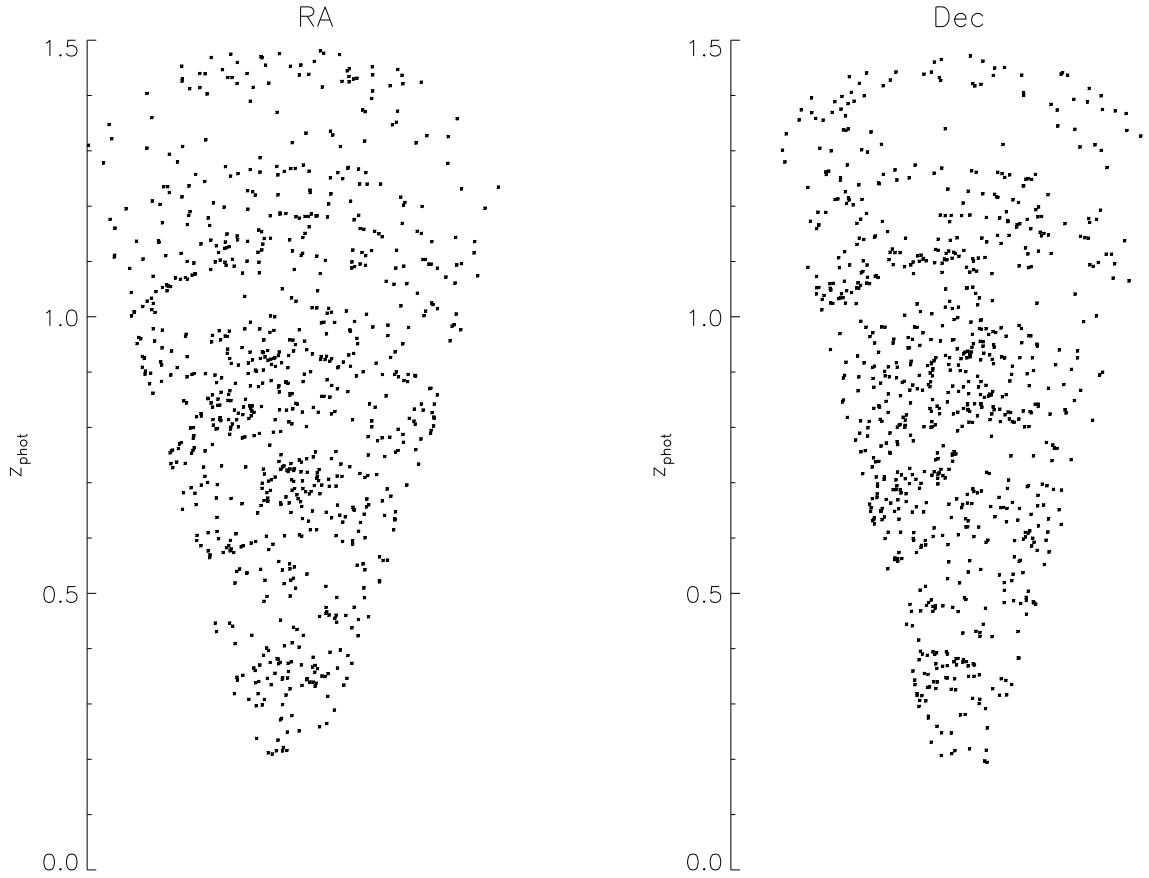

Figure 15. The large scale distribution of luminous galaxy clusters ($\log_{10}(\sum_{i=4} L_i/L_\odot) > 10.7$) galaxy clusters as the function of RA (left) and Dec (right) limited to $z_{ph} < 1.5$ objects.

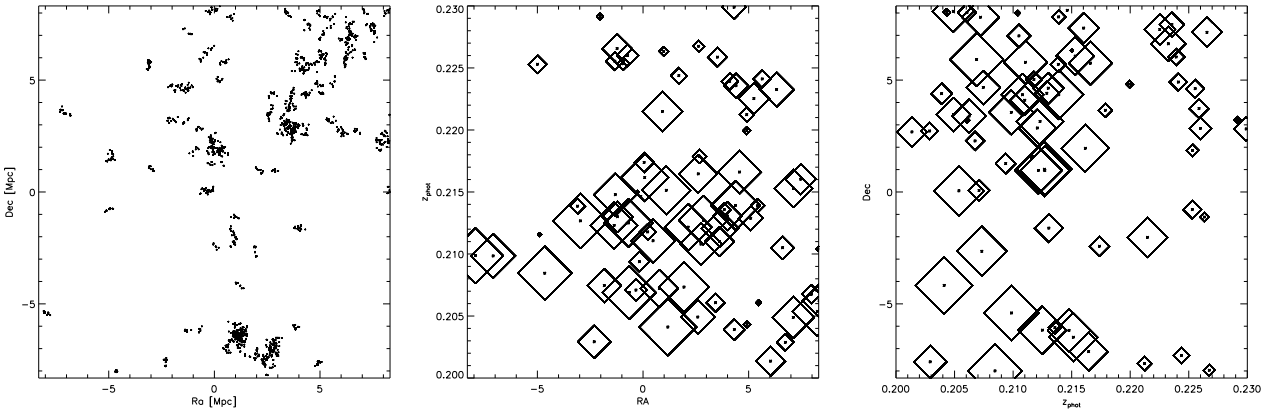

Figure 16. $z = 0.21$ pseudo supercluster. The left panel illustrates the distribution of all galaxies which are members of groups and clusters in the redshift range $0.20 < z_{ph} < 0.23$. The middle and right panel show the RA and Dec distribution of groups and clusters as function of redshift. The size of the plotting symbols in those two panels are proportional to $\log_{10}(\sum_{i=4} L_i/L_\odot)$ of the structures.

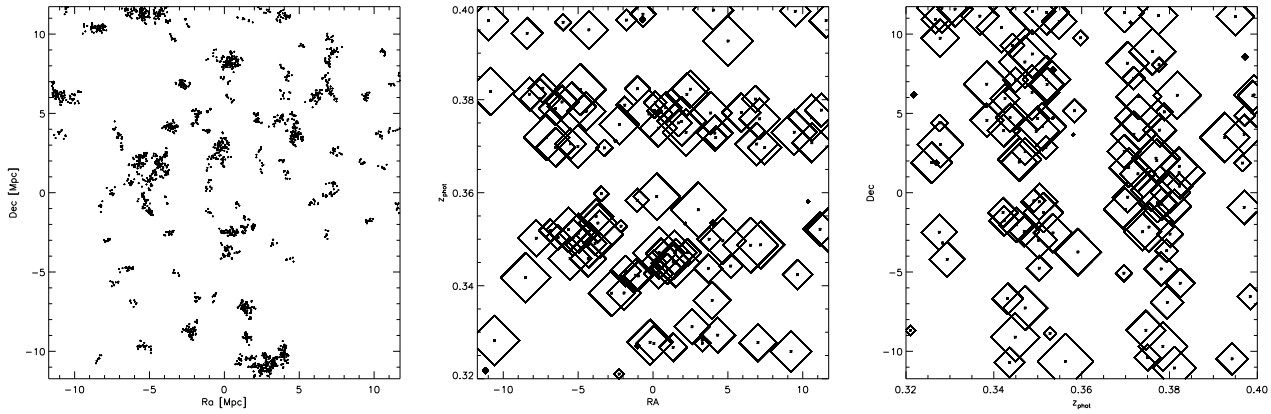

Figure 17. Possible double-layered supercluster. The left panel illustrates the distribution of all galaxies which are members of groups and clusters in the redshift range $0.32 < z_{ph} < 0.40$. The middle and right panel show the RA and Dec distribution of groups and clusters as function of redshift. The size of the plotting symbols in those two panels are proportional to $\log_{10}(\sum_{i=4} L_i/L_{\odot})$ of the structures.

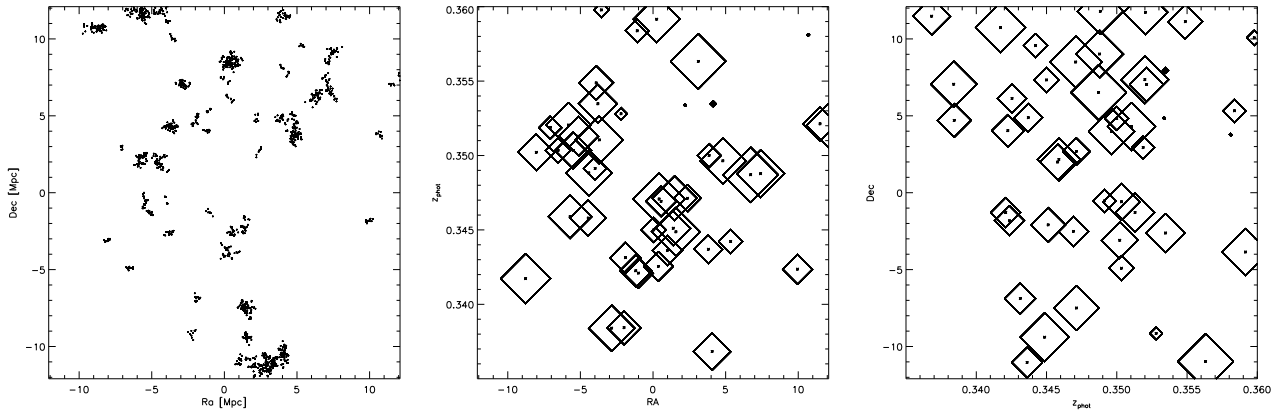

Figure 18. $z = 0.345$ component of the possible double-layered supercluster. The left panel illustrates the distribution of all galaxies which are members of groups and clusters in the redshift range $0.33 < z_{ph} < 0.36$. The middle and right panel show the RA and Dec distribution of groups and clusters as function of redshift. The size of the plotting symbols in those two panels are proportional to $\log_{10}(\sum_{i=4} L_i/L_{\odot})$ of the structures.

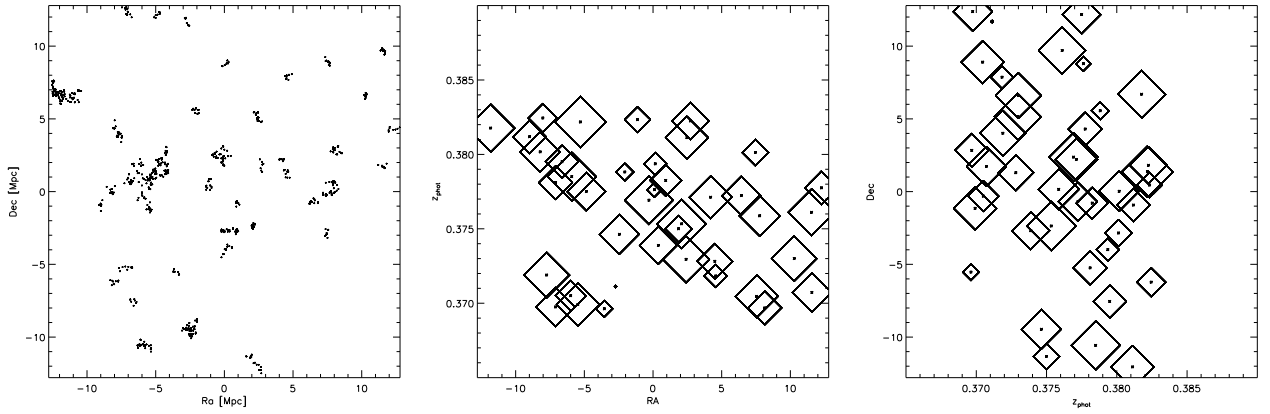

Figure 19. $z = 0.375$ component of the possible double-layered supercluster. The left panel illustrates the distribution of all galaxies which are members of groups and clusters in the redshift range $0.365 < z_{ph} < 0.390$. The middle and right panel show the RA and Dec distribution of groups and clusters as function of redshift. The size of the plotting symbols in those two panels are proportional to $\log_{10}(\sum_{i=4} L_i/L_{\odot})$ of the structures.

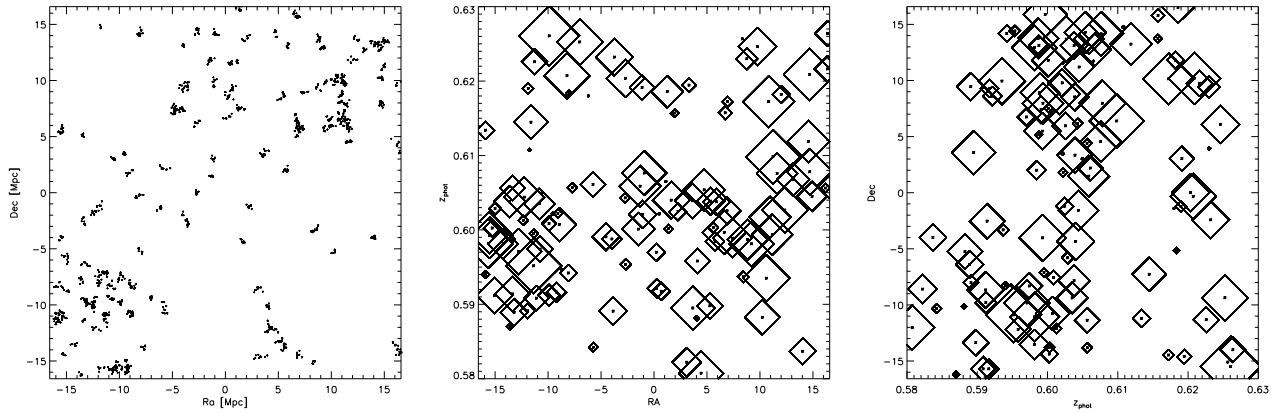

Figure 20. $z = 0.60$ pseudo supercluster. The left panel illustrates the distribution of all galaxies which are members of groups and clusters in the redshift range $0.58 < z_{ph} < 0.63$. The middle and right panel show the RA and Dec distribution of groups and clusters as function of redshift. The size of the plotting symbols in those two panels are proportional to $\log_{10}(\sum_{i=4} L_i/L_\odot)$ of the structures.

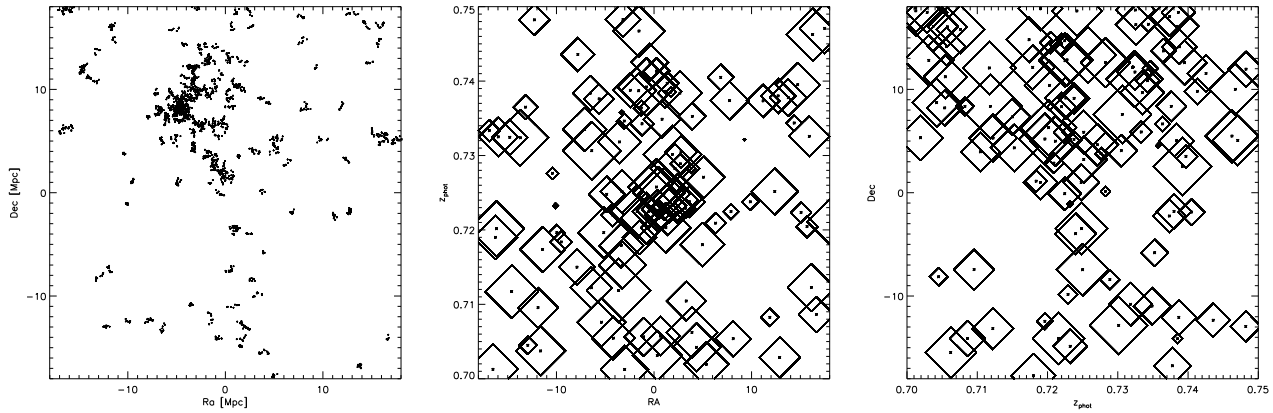

Figure 21. $z = 0.72$ supercluster. The left panel illustrates the distribution of all galaxies which are members of groups and clusters in the redshift range $0.70 < z_{ph} < 0.75$. The middle and right panel show the RA and Dec distribution of groups and clusters as function of redshift. The size of the plotting symbols in those two panels are proportional to $\log_{10}(\sum_{i=4} L_i/L_\odot)$ of the structures.

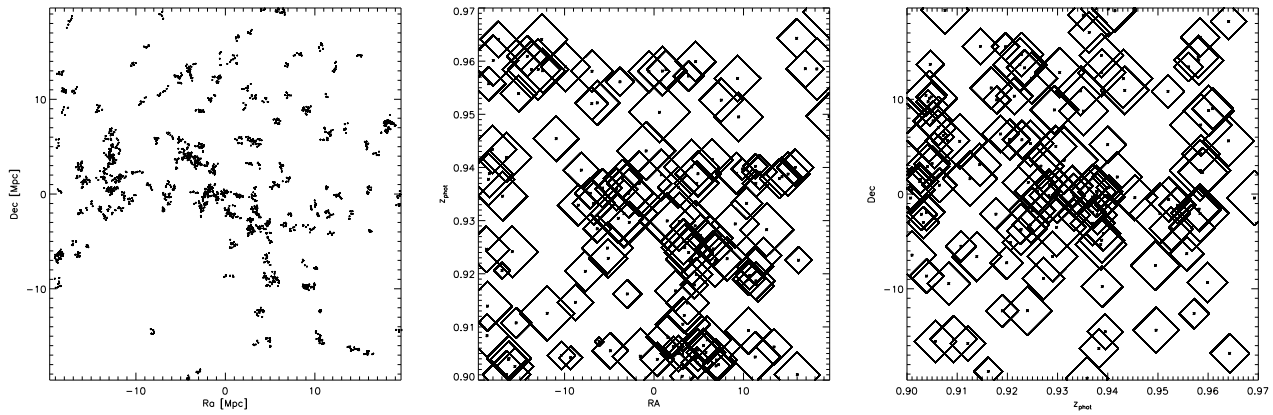

Figure 22. $z = 0.94$ supercluster. The left panel illustrates the distribution of all galaxies which are members of groups and clusters in the redshift range $0.90 < z_{ph} < 0.97$. The middle and right panel show the RA and Dec distribution of groups and clusters as function of redshift. The size of the plotting symbols in those two panels are proportional to $\log_{10}(\sum_{i=4} L_i/L_\odot)$ of the structures.

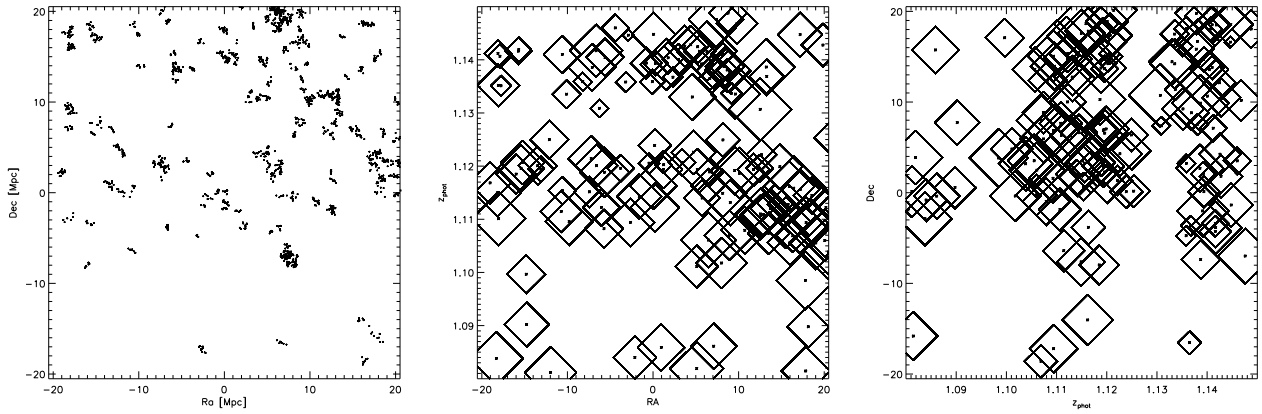

Figure 23. Possible double-layered supercluster. The left panel illustrates the distribution of all galaxies which are members of groups and clusters in the redshift range $1.08 < z_{ph} < 1.15$. The middle and right panel show the RA and Dec distribution of groups and clusters as function of redshift. The size of the plotting symbols in those two panels are proportional to $\log_{10}(\sum_{i=4} L_i/L_\odot)$ of the structures.

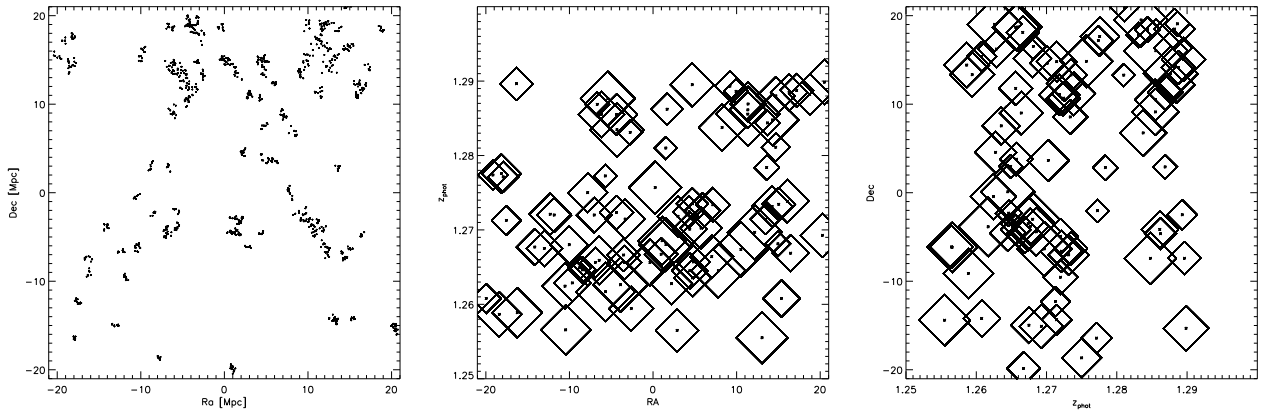

Figure 24. $z = 1.27$ supercluster. The left panel illustrates the distribution of all galaxies which are members of groups and clusters in the redshift range $1.25 < z_{ph} < 1.30$. The middle and right panel show the RA and Dec distribution of groups and clusters as function of redshift. The size of the plotting symbols in those two panels are proportional to $\log_{10}(\sum_{i=4} L_i/L_\odot)$ of the structures.

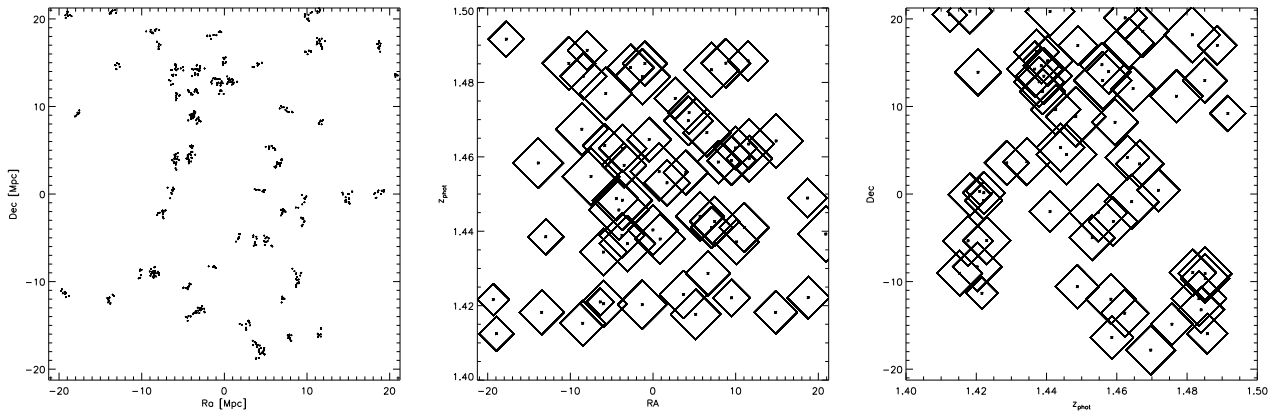

Figure 25. $z = 1.45$ supercluster. The left panel illustrates the distribution of all galaxies which are members of groups and clusters in the redshift range $1.40 < z_{ph} < 1.50$. The middle and right panel show the RA and Dec distribution of groups and clusters as function of redshift. The size of the plotting symbols in those two panels are proportional to $\log_{10}(\sum_{i=4} L_i/L_\odot)$ of the structures.

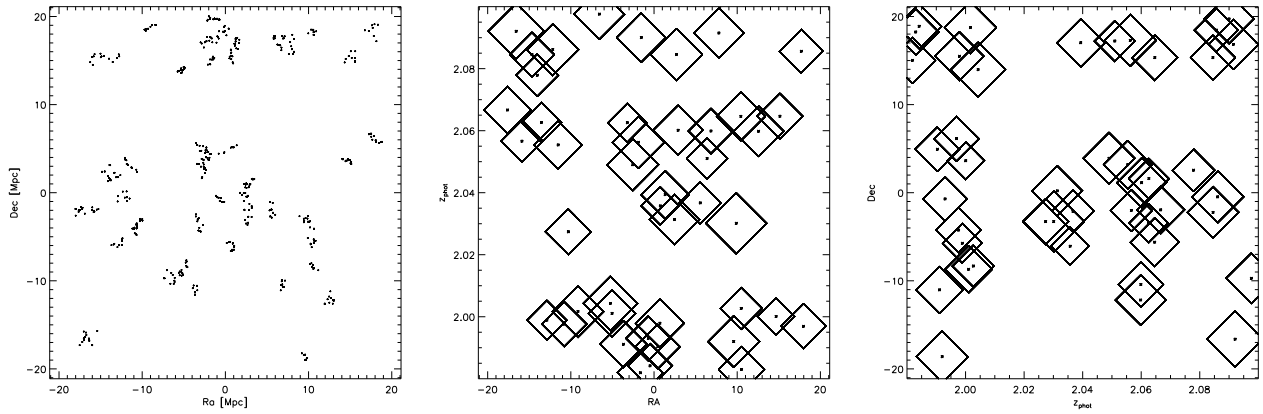

Figure 26. $z = 2.0$ supercluster. The left panel illustrates the distribution of all galaxies which are members of groups and clusters in the redshift range $1.98 < z_{ph} < 2.10$. The middle and right panel show the RA and Dec distribution of groups and clusters as function of redshift. The size of the plotting symbols in those two panels are proportional to $\log_{10}(\sum_{i=4} L_i/L_\odot)$ of the structures.

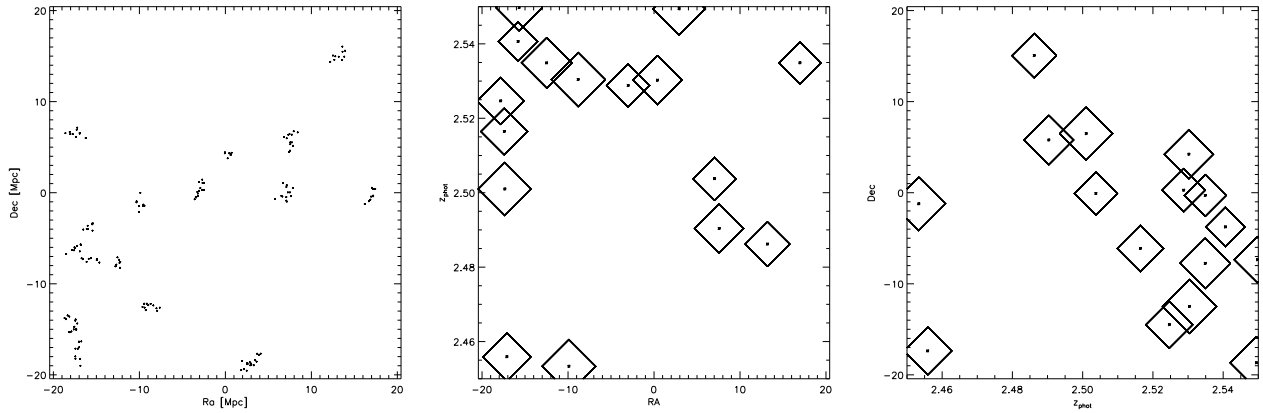

Figure 27. $z = 2.52$ supercluster. The left panel illustrates the distribution of all galaxies which are members of groups and clusters in the redshift range $2.45 < z_{ph} < 2.55$. The middle and right panel show the RA and Dec distribution of groups and clusters as function of redshift. The size of the plotting symbols in those two panels are proportional to $\log_{10}(\sum_{i=4} L_i/L_\odot)$ of the structures.

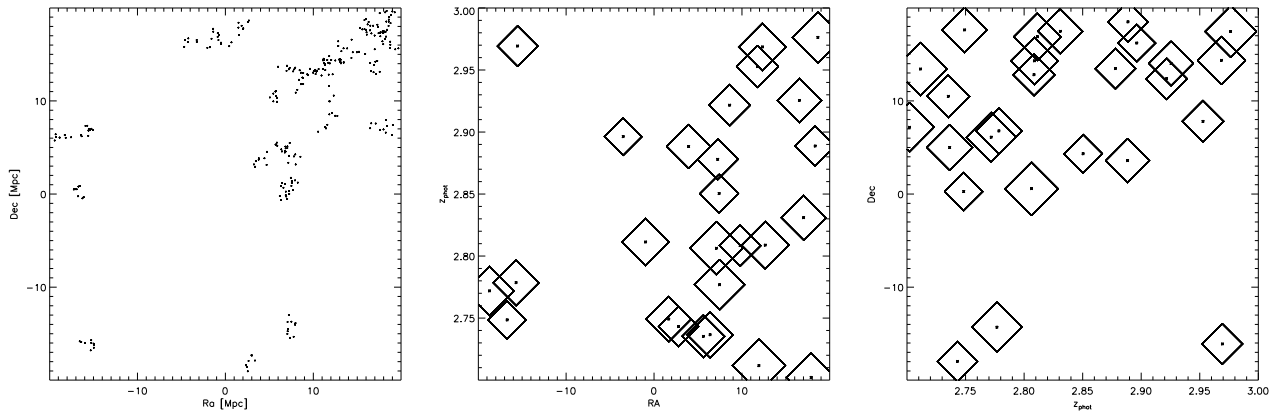

Figure 28. $z = 2.9$ supercluster. The left panel illustrates the distribution of all galaxies which are members of groups and clusters in the redshift range $2.70 < z_{ph} < 3.00$. The middle and right panel show the RA and Dec distribution of groups and clusters as function of redshift. The size of the plotting symbols in those two panels are proportional to $\log_{10}(\sum_{i=4} L_i/L_\odot)$ of the structures.

Table 1. The sample of 50 structures with the highest $\sum_{i=4} L$ detected in our study. The ID of the structure is the internal detection number. The RA and Dec are the mean coordinate of all the final member galaxies. The area of the structure is that enclosed by a convex hull around the voronoi cells of the final member galaxies. The richness is the number of the final cluster members derived from the magnitude restricted input catalogue (Figure 1). The number density is the richness divided by area. The $\sum_{i=4} L_i$ is the sum of luminosities of the four brightest galaxies in the K band.

ID	RA(J2000)	Dec(J2000)	z_{cl}	richness	area [Mpc^2]	number density [Mpc^{-2}]	$\sum_{i=4} L_i$ [$L_\odot$]
1003	149.9803162	2.326714039	0.931	184	15.0594	12.2183	3.64E+11
1333	150.1177979	2.007329941	1.179	19	18.4248	1.0312	3.28E+11
1336	149.8773956	2.875563145	1.184	19	11.6482	1.6311	3.23E+11
1501	150.1969299	2.577327251	1.37	8	2.1574	3.7082	3.23E+11
1014	150.0413513	2.188615799	0.937	165	18.755	8.7976	3.06E+11
1379	150.3041992	1.613412976	1.233	49	9.9823	4.9087	3.01E+11
925	149.9085999	2.672919035	0.885	138	16.374	8.428	3.00E+11
1208	150.6608276	2.835842371	1.116	28	27.6118	1.0141	2.89E+11
1122	149.7195129	2.256687403	1.017	226	10.8317	20.8646	2.88E+11
634	149.959137	2.524392366	0.712	649	21.3456	30.4043	2.86E+11
1407	150.4779205	2.733914137	1.286	131	4.6986	27.8806	2.84E+11
1701	150.5656738	2.852460146	2.187	10	1.1779	8.49	2.81E+11
1077	149.4965363	2.012138844	0.978	81	25.0924	3.2281	2.78E+11
1226	150.5270233	2.566051722	1.131	84	21.9926	3.8195	2.69E+11
827	150.5496368	2.199890852	0.832	91	22.7609	3.9981	2.63E+11
1098	149.5677948	2.080004931	0.98	50	11.8885	4.2057	2.53E+11
1045	150.7489471	2.459702015	0.959	63	26.4952	2.3778	2.51E+11
933	149.9377441	2.41486001	0.888	77	22.8025	3.3768	2.51E+11
1101	150.4177704	1.854271889	0.988	24	28.0257	0.8564	2.45E+11
343	149.4684143	2.426623821	0.481	176	29.9619	5.8741	2.44E+11
1631	150.0292358	2.249541998	1.835	11	2.0587	5.3432	2.43E+11
408	150.1854095	1.833799362	0.542	167	10.5147	15.8825	2.41E+11
862	149.6491241	2.372886419	0.837	40	15.0619	2.6557	2.41E+11
1136	149.9696655	1.534272432	1.019	63	13.1598	4.7873	2.39E+11
1042	149.6384583	2.288455963	0.958	139	14.5035	9.5839	2.38E+11
1044	150.1217804	2.127656698	0.95	45	18.1144	2.4842	2.36E+11
1666	150.4276276	2.091202021	2.03	14	6.7318	2.0797	2.36E+11
767	150.4052887	2.774184465	0.791	107	12.5656	8.5153	2.36E+11
867	150.5080261	2.228251696	0.834	42	32.5004	1.2923	2.34E+11
1624	149.7433319	2.107070446	1.798	40	2.671	14.9756	2.34E+11
558	149.682312	1.546154976	0.626	44	19.0215	2.3132	2.31E+11
1388	150.5143127	1.726904392	1.224	21	4.0522	5.1824	2.30E+11
1344	150.6403198	1.58499682	1.196	32	11.3951	2.8082	2.28E+11
860	149.5567627	2.420849323	0.835	28	17.0666	1.6406	2.25E+11
1529	149.9640808	2.348424196	1.446	30	13.0203	2.3041	2.25E+11
1209	150.3146057	2.864001274	1.142	199	22.5704	8.8169	2.23E+11
1522	149.9781342	2.491241455	1.448	37	15.3588	2.409	2.20E+11
919	150.0795441	2.534397841	0.885	97	25.4246	3.8152	2.18E+11
776	149.8401337	1.688799501	0.754	15	21.7762	0.6888	2.16E+11
414	150.3304749	1.654524803	0.527	91	11.3756	7.9996	2.15E+11
1645	149.9576721	1.941550136	1.953	11	3.5725	3.0791	2.13E+11
1420	149.9106903	2.071432114	1.262	16	22.6484	0.7065	2.12E+11
1310	150.3530121	2.086236	1.155	9	34.5623	0.2604	2.11E+11
815	150.5711823	2.644250631	0.799	38	12.7146	2.9887	2.05E+11
1039	150.0684509	2.633952618	0.943	30	29.9224	1.0026	2.04E+11
1100	149.8479614	2.587972641	0.987	43	16.909	2.543	2.02E+11
1023	150.2003326	2.074826479	0.93	47	23.9964	1.9586	2.01E+11
915	149.5543976	2.003553391	0.868	28	23.7841	1.1773	2.00E+11
1186	150.7076416	2.330537558	1.098	54	9.8976	5.4559	2.00E+11
694	150.0700684	2.298392534	0.739	157	21.8764	7.1767	1.97E+11

The $z = 0.21$ accumulation of structures, which we called a pseudo-supercluster, is very interesting in the sense that it is dominated by very compact groups, a fact also reported by Smolcic et al. (2007) for a smaller region of the COSMOS field. A further unique aspect is the appearance of poor but extremely dense groups consisting of lower luminosity galaxies. Due to the small area covered by the COSMOS field at $z = 0.21$, we are not able to distinguish conclusively if such exceptional groups are projections of filaments which, locally, are all aligned with the line of sight, or indeed if we are witnessing the advent of a new species of galaxy groups. Nevertheless, more suitable data sets are

available and we hope to resolve this puzzle in the future work.

We find a coherent structure beyond the scale of a single cluster at redshift $z \sim 2.9$, the most distant candidate for a precursor of today's superclusters. This is a sheet-like structure with a narrow filamentary projection in the spatial plane and a broader extent in the radial direction. All clusters in this structure harbour a large population of very bright galaxies suggesting a a high mass of the halo. This structure is an obvious target for a future follow up to establish its real extend in spatial and radial directions and also verify the membership of the bright clusters. Such accurate mapping of this early supercluster candidate should result in a reliable mass estimate of the member clusters and their likely M/L ratios aiding the studies of structure formation.

9 ACKNOWLEDGMENTS

We would like to acknowledge the use of the COSMOS data products. LEC acknowledges partial support from Center of Excellence in Astrophysics and Associated Technologies (PFB 06).

REFERENCES

Abell G. O., 1958, ApJS, 3, 211
Allard D., Fraley C., 1997, JASA, 92, 1485
Bahcall N. A., et al. 2003, ApJ, 585, 182
Bruzual A.G., Charlot S., 2003, MNRAS, 344, 1000
Carlstrom J.E., Holder G.P., Reese E.D., 2002, ARA&A, 40, 643
Colless M., et al., 2001, MNRAS, 328, 1039
Coziol R., Andernach H., Caretta C. A., Alamo-Martínez K. A., & Tago E., 2009, ApJ, 137, 4795
Dodd R. J., MacGillivray H. T., 1986, AJ, 92, 706
Einasto, M.; Liivamgi, L. J.; Tago, E.; Saar, E.; Tempel, E.; Einasto, J.; Martnez, V. J.; Heinmki, P., 2011, A&A, 532, 5.
Eke V.R., et al. 2004, MNRAS, 348, 866
Finoguenov A.., et al. 2007, ApJS, 172, 182.
Gladders M. D., Yee H. K. C., Majumdar S., Barrientos L. F., Hoekstra H., Hall P. B., & Infante L., 2007, ApJ, 655, 128
Gobat R., Daddi E., Onodera M., Finoguenov A., Renzini A., Arimoto N., Bouwens R., Brusa M., Chary R.R., Cimatti A., Dickinson M., Kong X., & Mignoli M., 2011, A&A, 526, A133
Ilbert O., et al. 2009, ApJ, 690, 1236.
Kepner J., Fan X., Bahcall N., Gunn J., Lupton R., Xu G., 1999, ApJ, 517, 78
Kim R. S. J., et al., 2000, in Mazure, Le Fèvre, Le Brun, ASP Conference Series, Vol. 200, p. 422
Knobel C., et al. 2009, ApJ, 697, 1842.
Longhetti M. & Saracco P., 2009, MNRAS, 394, 774
Lopes P. A. A., de Carvalho R. R., Gal R. R., Djorgovski S. G., Odewahn S. C., Mahabal A. A., Brunner R. J., 2004, AJ, 128, 1017
Miyazaki S., Hamana T., Ellis R.S., Kashikawa N., Massey R.J., Taylor J., Refregier A., 2007, ApJ, 669, 714
Maughan B.J., Jones C., Forman W., Van Speybroeck L., 2008, ApJS, 174, 117
Okabe A., Boots B., Sugihara K., Chiu S. N., 2000, Spatial Tessellations, 2nd edn. John Wiley & Sons
Padilla N., et al. 2004, MNRAS, 352, 211.
Padilla N., Lambas D. G., González R., 2010, MNRAS, 409, 936.
Pierre M., et al. 2006, MNRAS, 372, 591
Postman M., Lubin L., Gunn J. E., Oke J. B., Hoessel J. G., Schneider D. P., Christensen J. A., 1996, AJ, 111, 615
Ramella M., Boschin W., Fadda D., Nonino M., 2001, A&A, 308, 776
Romer A. K., Viana P.T. P., Liddle A. R., Mann R. G., 2001, ApJ, 547, 594
Rozo E., et al. 2009, ApJ, 708, 645
Schuecker P., Böhringer H., Collins C.A. & Guzzo L., 2003, A&A 398, 867
Scoville, N.Z., Abraham, R. G., Aussel, H. et al. 2007, ApJS, 172, 38.
Shectman S. A., 1985, ApJS, 57, 77
Smolĉic, V.; Schinnerer, E.; Finoguenov, A.; Sakelliou, I.; Carilli, C. L.; Botzler, C. S.; Brusa, M.; Scoville, N.; Ajiki, M.; Capak, P.; Guzzo, L.; Hasinger, G.; Impey, C.; Jahnke, K.; Kartaltepe, J. S.; McCracken, H. J.; Mobasher, B.; Murayama, T.; Sasaki, S. S.; Shioya, Y.; Taniguchi, Y.; Trump, J. R., 2007, ApJS, 172, 295
Söchting I. K., Clowes R. G., & Campusano L. E. 2002, MNRAS, 331, 569.
Söchting I. K., Clowes R. G., & Campusano L. E. 2004, MNRAS, 347, 1241.
Söchting I. K., Huber M.E., Clowes R. G., Howell S.B., 2006, MNRAS, 369, 1334.
Szabo T., Pierpaoli E., Dong F., Pipino A., Gunn J., 2011, ApJ, 736, 21.
Voit G. M., 2005, Reviews of Modern Physics, 77, 207
Weinberg, N.N., Kamionkowski M., 2002, MNRAS, 337, 1269
Zwicky F., Herzog E., Wild P., Karpowicz M., Kowal C. T., 1961–1968, Catalog of Galaxies and Clusters of Galaxies, in 6 vols., Pasadena, California Institute of Technology